Predicting Discharge from a Complex Karst System Using the Ensemble Smoother with Multiple Data Assimilation

Alessandro Pansa[1], Ilaria Butera[2], J. Jaime Gómez-Hernández[3], and Bartolomeo Vigna[4]

[1]Interateneo Department of Land Science, Planning and Policy, University of Turin, Italy. Email: alessandro.pansa@unito.it

[2]Department of Environment, Land and Infrastructure Engineering, Politecnico di Torino. Italy. Email: ilaria.butera@polito.it

[3]Institute for Water and Environmental Engineering. Universitat Politècnica de València. Spain. Email: jgomez@upv.es

[4]Department of Environment, Land and Infrastructure Engineering, Politecnico di Torino. Italy. Email: bartolomeo.vigna@polito.it

Abstract

Can the ensemble smoother with multiple data assimilation be used to predict discharge in an Alpine karst aquifer? The answer is yes, at least, for the Bossea aquifer studied. The ensemble smoother is used to fit a unit hydrograph simultaneously with other parameters in a hydrologic model, such as base flow, infiltration coefficient, or snow melting contribution. The fitting uses observed discharge flow rates, daily precipitations, and temperatures to define the model's parameters. The data assimilation approach gives excellent results for fitting individual events. After the analysis of 27 such events, two average models are defined to be used to predict flow discharge from precipitation and temperature, one model for prediction during spring (when snow melting has an impact) and another one during autumn, yielding acceptable results, particularly for the fall rainfall events. The lesser performance for the spring events may indicate that the snow melting approximation needs to be revised. The results also show that the parameterization of the infiltration

coefficient needs further exploration. Overall, the main conclusion is that the ensemble smoother could be used to define a characteristic "signature" of a karst aquifer to be used in forecast analyses. The reasons for using the ensemble smoother instead of other stochastic approaches are that it is easy to use and explain and provides an estimation of the uncertainty about the predictions.

1 INTRODUCTION

A quarter of the world population depends, partially or totally, on karst aquifers (Hartmann et al. 2015). Their importance is unquestionable, and many efforts have been made to understand their behavior and model them. One such effort is the vulnerability analysis done by (Banzato et al. 2017) using the VESPA method. But karst aquifers are very complex, and modeling their behavior is quite difficult (White 2003). One approach that has not been sufficiently explored in the study of karst aquifers is data assimilation algorithms. These algorithms have been successfully applied to solve environmental problems such as reverse flow routing identification (Todaro et al. 2019), hydrological problems (Khaki et al. 2020; Sun et al. 2020; Shokri et al. 2018; Bauser et al. 2018), contaminant source identification (Butera et al. 2021; Xu and Gómez-Hernández 2016; Chen et al. 2021; Gómez-Hernández and Xu 2022) or basin model building (Li et al. 2015). In this work, we studied the application of the ensemble smoother with multiple data assimilation (ES-MDA) to build a hydrological model for flow rate prediction in a karst aquifer using the well-known instantaneous unit hydrograph method (Sherman 1932) and the rational formula (Kuichling 1889), with the necessary adaptions to the specifics of the case study. The aquifer studied is the Bossea-Artesinera karst aquifer, located in northwest Italy, in the Maritime Alps (Civita et al. 1990).

To the best of the author's knowledge, the ensemble smoother has not been applied before in the hydrological modeling of a karst aquifer. Some of the challenges that have been addressed in the present work include the modeling of infiltration as a time-varying infiltration coefficient, the classification of precipitation into snowfall and rainfall, and the transformation of snow into water equivalent infiltration (this problem is well known, and many studies pointed out the relevance of the phenomenon in alpine karst aquifers, such as those by Lucianetti et al. (2020) or Jódar et al. (2020), but still, it remains an open issue (Oaida et al. 2019; Barnett et al. 2005)). The snow water-equivalent calculation follows an approach similar to the one in the Soil and Water Assessment Tool (Gassman et al. 2007; Uwamahoro et al. 2021), with a temperature-based identification of snowfall events and then an estimation of snow water equivalent infiltration during the melting period.

It is important to point out that the main objective of the paper is the stochastic analysis of flow discharges in a karst aquifer using real data. Many of the above-referenced works have demonstrated data assimilation approaches in synthetic datasets with few applications to real cases. In light of the successful applications in other environmental problems, this paper pretends to demonstrate that the ensemble smoother with multiple data assimilation can be applied for karst aquifer analyses providing meaningful predictions with associated uncertainty. As a secondary objective, this paper also builds a hydrological model —as complex as the limited available data allows— to relate precipitation, temperature, and discharge.

The ensemble smoother (ES) was introduced by Van Leeuwen and Evensen (1996) to solve inverse problems as an alternative to the ensemble Kalman filter (EnKF) with augmented state (Evensen 1994). Its main advantage is the assimilation of all observation data from all times at once, yielding more accurate estimates more efficiently than the EnKF, provided that the transfer function relating observation and model parameters is linear (Evensen 2003). For non-linear transfer functions, Emerick and Reynolds (2013) proposed the ensemble smoother with multiple data assimilation, which uses an iterative approach to assimilate the same data set multiple times, circumventing the problems related to non-linearities. A good description and comparison of several ensemble smoother methods can be found in Evensen (2018).

The paper is organized as follows: after the introduction, the ensemble smoother and the hydrological model are described; next, the case study is presented, and finally, results and discussions close the paper.

2 METHODS

2.1 Ensemble smoother with multiple data assimilation

The ensemble smoother with multiple data assimilation (ES-MDA) will be used in the context of inverse modeling to infer the parameters of a hydrological model from time observations of the state variables and forcing terms. The hydrological model is referred to as the system state transition equation or forward model in the data assimilation literature. In the context of the current paper, the forward model is a hydrological one that predicts discharge flow in a karstic aquifer from precipitation and temperature. The model is based on Sherman's instantaneous unit hydrograph (IUH) (Sherman 1932). The parameters describing the hydrological model are those defining the IUH plus the infiltration coefficient plus the parameters defining the snow water equivalent model needed to convert snow into infiltration. The forcing terms are precipitation and temperature, and the state variable is the time-varying flow discharge at the outlet. The state transition model is described in detail in the next section; for now and to describe the ES-MDA, it will be represented by the function g dependent on a vector of n model parameters $x \in \Re^n$. If the model parameters are known, the system state can be calculated as

$$y = g(x), \tag{1}$$

where $y \in \Re^m$ is a vector of predicted states uniquely determined by relation (1).

The purpose of the ES-MDA is to get an estimate of the parameter vector x from a set of observations

$$d = H \cdot g(x) + \epsilon, \tag{2}$$

where $d \in \Re^p$ is the subset of the system states that have been observed with some observation error ϵ (the error is assumed Gaussian distributed and with covariance R). The dimension of d does not have to coincide with that of y, that is, not all states need to be observed; matrix H is an observation matrix, generally composed of 0s and 1s, that extracts the subset of states that has been observed from the entire state vector y predicted by the forward model. In the hydrological model used in this manuscript, since the model predicts discharge at a single point —the outlet where it is observed— the dimensions of d and y are the same and equal to the number of time steps N_t at which flows are predicted/observed, (therefore, H is the identity matrix).

Estimating state parameters x proceeds in three steps: initialization, forecast, and update, of which the last two are iterated. This iteration is what gives the name of multiple data assimilation to the algorithm since each iteration amounts to re-assimilate all observations again to improve the last estimate of the parameters.

In the initialization process, an ensemble ($X^0 = [x_1, \ldots, x_{N_e}]$) of parameter vectors needs to be generated, its dimension being $\Re^{n \times N_e}$, with N_e being the number of ensemble members. All available prior information can and should be used in this procedure; the closer the initial values of the ensemble are to the real parameters, the better. Occasionally, there is little or no prior information, and the initial ensemble is generated from non-informative (uniform) distributions bounded between minimum and maximum values.

In the forecast step, the forward model (1) is used with each member of the ensemble of parameters X to generate an ensemble of predicted states $Y = [y_1 = g(x_1), \ldots, y_{N_e} = g(x_{N_e})]$, $Y \in \Re^{m \times N_e}$. The discrepancy between predictions and observations is used in the updating step.

The updating step —also known as the assimilation step since it is the step in which observations are brought in to improve the parameter estimates— uses the auto-covariance of the states C_{YY} and the cross-covariance between state and parameters C_{XY}. These covariances are estimated from the ensembles of parameters and state predictions by

$$C_{XY} = \frac{1}{N_e - 1}(X - \overline{X})(Y - \overline{Y})^T, \tag{3}$$

$$C_{YY} = \frac{1}{N_e - 1}(Y - \overline{Y})(Y - \overline{Y})^T, \tag{4}$$

where the overbar indicates ensemble mean. At the updating step, the number of multiple assimilations must have been already decided since they affect the updating equation as explained by Emerick and Reynolds (2013); let the number of assimilations be N_c. The update equation is

$$x_{j,i+1} = x_{j,i} + C_{XY}(C_{YY} + \alpha_i R)^{-1} \cdot (d + \sqrt{\alpha_i}\epsilon_j - y_j), \tag{5}$$

where j refers to the ensemble member and i refers to the assimilation step. After each assimilation, a new estimate of the parameters is obtained. The term $C_{XY}(C_{YY} + \alpha_i R)^{-1}$ is known as the Kalman gain. Parameter α_i is related to the number of assimilations and must satisfy the condition

$$\sum_{i=1}^{N_c} \frac{1}{\alpha_i} = 1. \tag{6}$$

A simple, commonly used solution is adopting $\alpha_i = N_c$. Different authors have proposed other methods, such as Evensen (2018) and Emerick (2019). The approach suggested by Rafiee and Reynolds (2017) has been used in this work.

The inbreeding problem. Inbreeding occurs when the filter collapses, that is, all ensemble members converge into a single realization with no variability among ensemble members. The topic is well known and has been discussed in the literature (Chen et al. 2021; Xu et al. 2013; Liang et al. 2012). The main reason behind inbreeding is a poor estimation of C_{YY} and C_{XY} by the experimental covariances given by (3) and (4).

This work has used two main approaches to avoid the inbreeding problem. The first one is the use of a damping factor, a number β between 0 and 1 that multiplies the gain in the update step as follows

$$x_{j,i+1} = x_{j,i} + \beta \cdot C_{XY}(C_{YY} + \alpha_i R)^{-1} \cdot (d + \sqrt{\alpha_i}\epsilon_j - y_j). \tag{7}$$

The second one is to apply covariance inflation. Among the alternative covariance inflation methods discussed in the literature (Bauser et al. 2018; Anderson 2007; Wang and Bishop 2003), the one proposed by Anderson and Anderson (1999) has been chosen after some tests. The selected method uses a coefficient λ greater than one —to be chosen by trial and error— to spread the updated parameter values around their mean value, effectively increasing their variance. After each updating step (7), the parameter values are modified according to

$$\dot{X}_j = \lambda \cdot (X_j - \bar{X}_j) + \bar{X}_j \tag{8}$$

where the overbar refers to the mean value and the dot to the modified update.

2.2 Hydrological Model

The hydrological model is based on the convolution of an instantaneous unit hydrograph with the inflow calculated using a modified rational formula (Kuichling 1889) to account for snow melting. In addition, an initial base flow Q_b is also considered. Many authors highlighted the importance of the snowmelt contribution to aquifer recharge, such as Lucianetti et al. (2020) and Jódar et al. (2020), whose studies dealt with karst systems in alpine and pre-alpine areas. Bittner et al. (2021) also highlights the influence that the uncertainty associated with snowmelt models exerts on the modeled discharge. However, in this work, in the absence of distributed data measurements, snow melting is an unknown to be estimated by the model, driven by simple empirical relationships as described next. Trying to use a more sophisticated model does not make sense, and, besides, it is not the main focus of the paper.

The equation for the rational method is

$$I(t) = \chi(t) \cdot A \cdot (i(t) + Sn(t)), \tag{9}$$

where $I(t)$ $[L^3T^{-1}]$ is the total infiltration into the aquifer $\chi(t)$ $[-]$ is a time-varying infiltration coefficient, A $[L^2]$ is the recharge area, $i(t)$ $[LT^{-1}]$ is the observed rainfall and $Sn(t)$ $[LT^{-1}]$ is the snowmelt contribution.

Computing the snowmelt contribution to infiltration faces two challenges. First, there is a need to know whether the precipitation registered at the gauge (a heated gauge) corresponds to snow or rain. Second, snow accumulates and slowly releases when the temperature is above freezing.

After several trial-and-error runs, the following logical expression was derived to classify precipitation into snow or rain

$$\begin{aligned} snow =&(T_{min}^{mm} \leq -1 \vee T_{avg} \leq 1 \vee T_{avg}^{mm} \leq 0 \vee T_{max} \leq 4 \vee T_{min} \leq 1.5)\wedge \\ &\wedge (T_{min} \leq 0 \vee T_{min}^{mm} \leq -1), \end{aligned} \tag{10}$$

where all values are in Celsius degrees, T_{min} is the minimum daily temperature, T_{avg} is the average daily temperature, T_{max} is the maximum daily temperature, and T_{min}^{mm} and T_{avg}^{mm} are the minimum and average values of the temperature moving average over three days; when this expression is true, the precipitation fallen is snow.

To calculate the snow water equivalent infiltration, a release function of time is constructed that takes into account the total precedent fallen snow according to the following expressions

$$Sn'(t) = \frac{\Sigma_s}{2\sqrt{2\pi b_1^2}} \cdot e^{-\frac{(t-a_1)^2}{2b_1^2}} + \frac{\Sigma_s}{2\sqrt{2\pi b_2^2}} \cdot e^{-\frac{(t-a_2)^2}{2b_2^2}}, \tag{11}$$

$$Sn(t) = \frac{Sn'(t)}{\sum_{t=1}^{N_T} Sn'(t)} \cdot V_s, \tag{12}$$

where Σ_s $[L]$ is the cumulative snow-equivalent precipitation measured at the gauge and a_1, b_1, a_2, b_2 are parameters subject to identification during the inversion process; the intermediate values $Sn'(t)$ $[LT^{-1}]$ are normalized so that the total snow melting (as snow-water equivalent) matches the observed value of fallen snow-equivalent precipitation V_s $[L]$. The total number of days simulated is N_T. Notice that snow infiltration happens only when snow is on the ground, and the temperature is above 0 °C. Fig. 1 shows a typical result of snow water equivalent computed by this approach. In dark blue, both the daily snow precipitation and the cumulative precipitation during the first half of the year 2012 are shown, and, in light blue, the melted snow (both daily and accumulated) lagging in time with the fallen snow but accumulating to the same total by the end of May 2012.

The infiltration is routed to the outlet using the following kinematic equation that provides the flow discharge

$$Q(t) = \int_0^t I(t) \cdot h(t-\tau) d\tau, \tag{13}$$

where $Q(t)$ $[LT^{-3}]$ is the discharge flow and $h(t)$ $[-]$ is the instantaneous unit hydrograph (IUH) to be subject to identification during the inversion process. The shape of the IUH is parameterized with the following expressions

$$h'(t) = \frac{1}{\sqrt{2\pi v_1^2}} \cdot e^{-\frac{(t-m_1)^2}{2v_1^2}} + \frac{1}{v_2} \cdot e^{-\frac{t}{m_2}}, \tag{14}$$

$$h(t) = \frac{h'(t)}{\sum_{t=1}^{N_T} h'(t)}, \tag{15}$$

where v_1, m_1, v_2, m_2 are parameters to be identified during the inversion process. The intermediate values $h'(t)$ are normalized to ensure that the area under the IUH equals 1.

Replacing (9) into (13) and considering that there could be an antecedent base flow due to previous rainfall, the final equation that models the routing of the precipitation into discharge is

$$Q(t) = Q_b(t) + \int_0^t [\chi(t) \cdot A \cdot (i(t) + Sn(t))] \cdot h(t-\tau) d\tau, \tag{16}$$

where Q_b $[LT^{-3}]$ is the base flow, which will be assumed to decay exponentially as

$$Q_b(t) = Q_g(0) \cdot e^{-q_2 \cdot t}, \tag{17}$$

where $Q_g(0)$ is the flow at the gauge at the beginning of the period analyzed and q_2 $[T^{-1}]$ is a decay rate to be identified during the inversion process.

The hydrological model is thus established. Its parameters are the four parameters defining the snow melting equation, the four parameters defining the unit hydrograph, the decay coefficient for the base flow, plus the daily infiltration coefficients. All these parameters will be subject to identification during the inversion process by ES-MDA. Since the updating equation (7) does not ensure that the updated values will be constrained within specified limits, the ES-MDA is applied to some transform of some of the variables: to ensure that the decay rate q_2 is always positive, the ES-MDA works with its logarithm, and to ensure that the infiltration coefficients are between 0 and 1, the following transformation is used

$$\chi'(t) = \frac{1 - \chi(t)}{\chi(t)}. \tag{18}$$

The input data will be temperatures and precipitations, and the output will be flow discharge. An example of the input data and the observed discharge for an event occurring in the spring of 2012 is shown in Fig. 2.

More complex hydrological models could have been considered, including explicitly processes such as evapotranspiration or interception and even distributing the parameters in space; however, there are no data that would justify the construction of such a model. For this reason, the infiltration model depends only on an infiltration coefficient that lumps together all the processes affecting rainfall until it becomes net inflow into the aquifer; and the routing model is based on the unit hydrograph. The snowmelt component had to be modeled aside; our preliminary tests showed that this process could not be lumped into the infiltration coefficient. The final model for the snow-equivalent infiltration was the simplest one possible (depending only on four parameters) and capable of reproducing the dynamics of snow melting at the site.

3 CASE STUDY

The system analyzed in this work is the Bossea-Artesinera karst aquifer. It is located in Northwest Italy, in the Maritime Alps district, and it is a rather complex karst system, well studied and described by Antonellini et al. (2019). In Fig. 3, the study area location is shown. Part of the system is accessible through the Bossea Cave. The infiltration basin covers around 6 km^2, as indicated by Civita et al. (1990), which is the value used in the model. The entrance to the cave opens onto the middle Corsaglia valley, through which the stream of the same name flows. The primitive glacial morphology has almost disappeared due to the intense erosion by the watercourse. This strong erosion has two main causes: a change in the base level of the Tanaro river, of which the Corsaglia is a tributary, and a recent uplift of the entire Alpine sector where the aquifer is located. Towards the west of the basin, the karst absorption areas open up, consisting of valleys dug by the erosion of temporary waterways. An alternation of waterproof quartzites can be identified, replaced by limestone where the water infiltrates to reach the aquifer. Karst soils are partially covered by insoluble residues on which vegetation grows. Towards Prato Nevoso, the landscape turns into gentler karst forms with a grassy cover, where there are some absorbent sinkholes.

The climate is strongly influenced by the nearby Mediterranean Sea (about 40 km away) with abundant rainfall in autumn, generally in November, and in spring, typically in May, while the driest season is summer. The mountainous environment leads to frequent snow falling in the cold months, especially in the higher part of the basin, which rises to 2382 m.a.s.l. The winter is mainly characterized by freezing temperatures, especially at night, and snow precipitations. For these reasons, a second dry season occurs during the winter. Concerning snowfall, a maximum height of snow during the season can be found between 50 cm and 250 cm, usually recorded in the late winter period. There is often a remarkable difference in precipitation between the lower and the higher areas. The snow melting lasts for the entire springtime, starting in March and continuing until May. It affects first the sunny slopes, usually east and south, and then those in the shade, north and west, through the whole spring. The mean annual precipitation calculated during 2001-2018 is equal to 1372 mm with a standard deviation of 381 mm, indicative of a large variability across the years.

Data are gathered in two different locations: the Borello weather station, managed by ARPA Piemonte, where there are an air thermometer and a heated gauge able to measure rainfalls and snow falling as millimeters of water; and the Bossea Scientific Station inside the cave, managed by the Italian Alpine Club and Turin Polytechnic, where the outgoing flow rate is measured with a weir located on the stream crossing the Bossea Cave. The weir is placed after a pool of calm water more than 100 m long, allowing to take measurements with a precision of 1 Ls^{-1}. The data analyzed cover from 2001 to 2018. In Fig. 3, the aquifer basin, the Borello weather station, and the cave entrance —where flow rates are measured— are shown.

4 RESULTS

Two exercises have been performed. The first one is fitting: given the information of an event such as that in Fig. 2, can the parameters of the hydrological model be identified by the ES-MDA?

With which degree of uncertainty? The second is a forecasting one: once several events have been fitted, can a unique set of parameters be extracted from the analysis of all fits that could be used to forecast flow rates given input precipitations and temperatures?

At the end of either exercise, there is not a single prediction of the parameter values but an ensemble of values for each parameter. This ensemble allows retrieving one value as the best estimate —it could be the mean or the median, for example— and also a measure of uncertainty given by the spread of values and summarized by, for instance, the standard deviation or a confidence interval. Such uncertainty about the predictions should not be confused with the expected time variability of the discharge; instead, it measures the amount of information in the dataset and how reliable forecasts are.

4.1 Fitting

The ES-MDA was applied first to fit the event observed during the spring of 2012. The input data is shown in Fig. 2 and is discretized daily. The ES-MDA is run with 15 data assimilations, that is, $N_c = 15$, and with 1000 ensemble members, that is, $N_e = 1000$. The hydrologic model is run with daily frequency. The parameter vector that has to be identified by the ES-MDA is the following

$$x = [m_1, v_1, m_2, v_2, a_1, b_1, a_2, b_2, \chi'_1, \chi'_2, \ldots, \chi'_{N_T}, q'_2], \tag{19}$$

where N_T is the duration in days of the event being analyzed, the prime marks indicate that the ES-MDA is not applied to the parameters themselves but rather to a transformation of them, as explained earlier. Just as a recall, the first four parameters serve to define the parametric shape of the IUH, the next four parameters control the snow water equivalent model, the next N_T parameters are the daily infiltration coefficient transforms, and the last parameter is the logarithm of the decay rate of the base flow.

The initial ensemble of realizations is generated by drawing, independently, each value from the following uniform distributions, m_1 and m_2 from $\mathcal{U}[1, 5]$, v_1 and v_2 from $\mathcal{U}[5, 10]$, a_1, b_1,

a_2, b_2 from $\mathcal{U}[5, 10]$, ξ_i from $\mathcal{U}[0, 1]$ and q_2 from $\mathcal{U}[0, 0.5]$. The ranges of the parameters were chosen based on prior information or by trial and error as good starting points for the assimilation algorithms. Particularly, the IUH parameters were guided by previously performed tracer tests. In any case, the algorithm itself updates the parameter values at each assimilation step without any constraint on the interval over which the parameters may fall; that is, the range of the initial set of parameters has only a marginal influence on the final solution given by the ES-MDA. After the drawing, infiltration and decay coefficients are transformed as indicated in subsection 2.2. To prevent filter inbreeding, a damping factor of 0.38 and a covariance inflation of 1.12 were used (again, these two parameters were chosen by trial and error).

Figure 4 shows the ensemble of initial daily infiltration rates and the ensemble of initial IUHs built with the values drawn for m_1, v_1, m_2, v_2 from their corresponding distributions. As noted, these initial values display a wide variability.

The results of the inversion for the data in Fig. 2 are shown in Fig. 5 where the one thousand final IUHs and the one thousand final daily infiltration coefficients are shown. Also, the infiltration coefficient ensemble average is shown in red. There is little uncertainty about the final IUH, whereas the uncertainty about the infiltration coefficients is larger, particularly during the spans when there is little or no infiltration.

Next, the performance of the inverted values is analyzed by predicting the discharge flow rates using these values. Recall that the ES-MDA does not provide a single answer but an ensemble of answers. When each of these answers is plugged into the hydrological model, and the model is run, the resulting flow rates compare pretty well with the observed ones, as seen in Fig. 6. This figure shows, with a dotted line, the observed flow rates, and with a yellow band, the results obtained with the ensemble of inverted parameters; the red line is the ensemble average. The reproduction is quite good except for a few spans, probably due to failure in predicting the snow water equivalent. The figure also shows, for reference, the base flow in green and the computed average snow water equivalent precipitation.

Besides the visual comparison of predictions versus observations, several performance indicators have been computed: the Nash-Sutcliffe efficiency coefficient (NSE) (Nash and Sutcliffe 1970), the percentage of total volume error, the average bias in flow prediction, and the root mean square error. The expressions for these indicators are given below.

Nash-Sutcliffe efficiency

$$NSE = \frac{\sum_{t=1}^{N_T}(Q_o(t) - Q_m(t))^2}{\sum_{t=1}^{N_T}(Q_o(t) - \bar{Q}_o)^2} \quad (20)$$

where $Q_o(t)$ are the observed (daily) flow rates, $Q_m(t)$ are the median values of the ensemble of modeled daily flow rates and $\bar{Q}_o$ is the mean of the measured flow rates. The summation extends over all the days modeled, N_T.

Percentage volume error

$$VolRelErr(\%) = \frac{V_o - V_m}{V_o} \cdot 100 \quad (21)$$

where V_o is the volume computed by integrating the discharge curve of observed flow rates and V_m is the volume calculated by integrating the median values of the ensemble of modeled flow rates.

Average bias

$$Bias = \frac{1}{N_T}\sum_{t=1}^{N_T}(Q_m(t) - Q_o(t)) \quad (22)$$

Root mean square error

$$RMSE = \sqrt{\frac{1}{N_T}\sum_{t=1}^{N_T}(Q_m(t) - Q_o(t))^2} \quad (23)$$

For this specific case, the resulting values of these indicators can be seen in Table 1.

Regarding potential filter inbreeding, the evolution of the ratio between the root mean square error (RMSE) and the average ensemble spread (ES) has been computed for the observed and predicted values of the spring 2012 event. The RMSE is calculated, for each day, using Eq. (23), and the ES is given by

$$ES = \frac{1}{N_T} \sum_{t=1}^{N_T} \sigma_t \tag{24}$$

with σ_i being the standard deviation of the flow model predictions at a given time t. Figure 7 shows the evolution of both RMSE and RMSE/ES with the number of data assimilations. While the RMSE measures the prediction error, the ES measures the fluctuation of the predictions around the mean prediction. Desirably the ratio RMSE/ES should be around 1, indicating that there is no filter inbreeding. In the spring 2012 event, the RMSE gets as low as 14 $\mathrm{L\,s^{-1}}$ after 15 assimilation cycles, but still, it is 3.5 larger than the ES. While the ratio RMSE/ES is larger than 1, its value is not disproportionate. It cannot be considered an indication of filter inbreeding since much of the RMSE value is due to the estimation bias reported in Table 1.

4.2 Forecasting

The above fitting procedure was performed for all 27 identified events in the 2001-2018 year span. Their analysis shows some recurrent behavior that points towards a possible aquifer signature, which could be used for forecasting.

The first thing that could be noticed is that the aquifer response is different in the first half of the year (spring) than in the second half (autumn). Therefore, if such a signature exists, it will differ depending on the season.

Next, an average response is extracted from the analysis and then used to forecast a couple of events, one in each season.

Figure 8 shows the average IUHs from the ensemble of realizations resulting after fitting all events happening in spring between 2001 and 2018. All IUHs show similar behavior, except for spring 2011, which shows a bump around day 20. Two alternatives are proposed for a representative IUH for spring events at the Bossea aquifer: (i) to use the IUH obtained with the average value of the parameters m_1, v_1, m_2, v_2, (solid red line in the figure), or (ii) consider the average of the IUHs in the figure, and then find the best fitting parameters for m_1, v_1, m_2, v_2 to this average IUH (dashed red line in the figure). After some tests trying to forecast individual events, it was found that the second option is the one that works best and is retained.

Similarly, Fig. 9 shows the average IUHs from the ensemble of realizations resulting after fitting all events happening in the summer/fall between 2001 and 2018. The similarity among the IUHs is larger than for the spring ones. The same two options to obtain a mean representative IUH were considered, although the difference between the solid red line (IUH with average parameters) and the dashed red line (IUH fitted to the average of the individual IUHs) is small.

As already mentioned, the representative IUH differs depending on the season. The spring hydrograph distributes the discharge over a more extended period. In contrast, the autumn hydrograph is more explosive, with most flow occurring a few days after precipitation falls.

Regarding the infiltration coefficients, Fig. 10 shows a statistical summary of the daily infiltration coefficients over the calendar year obtained during the fitting exercise to all the events: in red, the mean value, and in blue, the interval given by the average plus-minus one standard deviation. Overall, the uncertainty about the infiltration coefficient is significant, but some clear trends are observed; the infiltration coefficient peaks at the beginning of spring and has the lowest values once fall has started, with a second lower peak in early December. The mean coefficients in the figure are the ones chosen to forecast.

The analysis of the snow melting parameters a_1, b_1, a_2, b_2 does not show any noticeable trend. The only conclusion drawn is that a Gamma distribution could fit the resulting values. Their median values have been chosen for the forecast.

Finally, the decay coefficient q_2 used to describe the base flow does not show any pattern either, and its median value is chosen for the forecast.

Having selected the representative parameters of a generic hydrological model for the Bossea aquifer, the forecast of some observed events is performed without any additional fitting or parameter adjustment. Figures 11 and 12 show the forecast for the spring 2013 event and for the fall 2016 event, respectively. These figures display, as a dashed black line, the observed discharges and, as a solid red line, the forecast obtained using the representative parameters described above. Also, the two solid purple lines show the predictions using the infiltration coefficients from the upper and lower curves in Fig. 10. For completeness, both figures also show the base flow in green and the rainfall and snow equivalent precipitations in dark blue and light blue, respectively.

For it being a blind prediction, the results can be considered acceptable, especially for the fall event. The existence of a “signature" IUH was clearer for the fall events (see Fig. 9) than for the spring events (see Fig. 8). The NSE and the error in total flow calculation have been computed for the red and purples lines in Figs. 11 and 12 and are reported in Tables 2 and 3, respectively. The NSE, as expected, is much better (closer to 1) for the fall event than for the spring event, although the error in total volume prediction is the opposite.

5 DISCUSSION AND CONCLUSIONS

This paper explores the possibility of identifying the parameters describing a hydrological model for an Alpine karst system using the ensemble smoother with multiple data assimilation (ES-MDA). For this purpose, a model coupling the rational method with time-varying infiltration coefficients, the instantaneous unit hydrograph, and a snow water equivalent precipitation calculation has been built. The method has been tested using data from the Bossea aquifer in Italy. Despite having only one meteorological station, the simple black-box-type model can provide discharge predictions that match the observed values at the discharge flow gaging station.

The model has demonstrated its ability to route precipitation onto flow discharge when the parameters describing it are fitted using the input precipitation and temperature, and the output discharge as known. These results demonstrate, again, the efficiency of the ensemble-based filters and smoothers for inverse modeling. Some of the advantages of the ES-MDA are that it considers all data for all times at once and that, being an ensemble-based method, it always provides an ensemble of final results from which best estimates for the parameters (such as the mean or the median) and uncertainty bounds (such as the standard deviation or the interquartile range) can be extracted; also, the ES-MDA is conceptually simple to explain and very fast in its implementation.

Although only one such fit is shown in the paper, the fits corresponding to other events are equally good, with NSE values never below 0.9, in most cases, above 0.95. The conclusion that could be drawn from this fitting exercise is that, indeed, the ES-MDA can be used to fit a hydrological model of the kind described in this paper.

Then, the question remained of whether a single set of parameters could be deduced from the fitting of the different events that would be representative of the aquifer and could be used for forecasting purposes. The different events had to be split into two sets since it was clear that the response of the aquifer was not the same during spring (with substantial amounts of infiltration coming from snow melting) as during autumn when the observed response was more explosive and closer to a fast flood. After the splitting, average values were computed from the individual event fittings, and an average model was formulated for each season.

Using these average models for predictions did not work as remarkably as the individually fitted models. There is a need to analyze further why this happened and ways to improve the results. The comparison of the spring and fall models results in a better assessment of the fall model, which may indicate a need to reevaluate the implementation of the snow equivalent calculation since this is the main difference between the two seasons.

Another item that may need reevaluation is the time-varying infiltration coefficients. Initial investigations using a constant infiltration coefficient did not work, meaning that an accurate forecast can only be obtained with infiltration coefficients that vary in time. The average model presented in Fig. 10 shows a clear cyclic trend over the natural year but also displays too much short-scale variability. There is a need to explore alternative parameterizations for the infiltration coefficient, maybe accounting for antecedent precipitation.

The analysis of Fig. 11 shows that the model forecasts too much flow in response to the March and April precipitations. The first observed peak discharge may be due to snowmelt and is not fully captured by the model. Then the final recession curve (starting in June 2013) corresponds to an aquifer with a larger storage volume than the one implied by the forecasting model.

The analysis of Fig. 12 is more favorable, and the observed discharge is almost perfectly reproduced by the predicted one using the average model.

It is necessary to highlight that the area of the infiltration basin is but a rough estimation and that a better definition of it could yield more reliable results.

It is difficult to conclude whether a signature response can be built for the Bossea aquifer. Still, it is clear that the ES-MDA is a powerful tool to fit individual events, which could be used to better understand the dynamics of the complex Bossea karst system. An interesting continuation of this work would be using the ES-MDA to fit a unique hydrological model to all data for all events simultaneously. Such an approach could identify that elusive unique response that was not fully characterized in this work.

6 ACKNOWLEDGMENTS

The authors would like to thank the Bossea Cave Scientific Laboratory personnel and ARPA Piemonte for the many years of work spent maintaining the instrumentation, collecting data, and sharing the data.

7 STATEMENTS & DECLARATIONS

7.1 Funding

J. Jaime Gómez-Hernández acknowledges grant PID2019-109131RB-I00 funded by MCIN/AEI/10.13039/5011

7.2 Competing interests

The authors have no relevant financial or non-financial interests to disclose.

7.3 Author contributions

All authors contributed to the study's conception and design. Model construction, model runs, and preliminary analyses were performed by Alessandro Pansa, who also wrote the first draft of the manuscript. All authors commented on and edited the several versions until the current one. All authors read and approved the final manuscript.

7.4 Data availability

The data supporting this study's findings are available from the corresponding author upon reasonable request.

References

Anderson, J. L. (2007). "An adaptive covariance inflation error correction algorithm for ensemble filters." *Tellus A: Dynamic Meteorology and Oceanography*, 59, 210–224.

Anderson, J. L. and Anderson, S. L. (1999). "A monte carlo implementation of the nonlinear filtering problem to produce ensemble assimilations and forecasts." *Monthly Weather Review*, 127, 2741–2758.

Antonellini, M., Nannoni, A., Vigna, B., and Waele, J. D. (2019). "Structural control on karst water circulation and speleogenesis in a lithological contact zone: The bossea cave system (western alps, italy)." *Geomorphology*, 345, 106832.

Banzato, C., Butera, I., Revelli, R., and Vigna, B. (2017). "Reliability of the vespa index in identifying spring vulnerability level." *Journal of Hydrologic Engineering*, 22(6), 04017008.

Barnett, T. P., Adam, J. C., and Lettenmaier, D. P. (2005). "Potential impacts of a warming climate on water availability in snow-dominated regions." *Nature*, 438(7066), 303–309.

Bauser, H. H., Berg, D., Klein, O., and Roth, K. (2018). "Inflation method for ensemble kalman filter in soil hydrology." *Hydrol. Earth Syst. Sci.*, 22, 4921–4934.

Bittner, D., Richieri, B., and Chiogna, G. (2021). "Unraveling the time-dependent relevance of input model uncertainties for a lumped hydrologic model of a pre-alpine karst system." *Hydrogeology Journal*, 29(7), 2363–2379.

Butera, I., Gómez-Hernández, J. J., and Nicotra, S. (2021). "Contaminant-source detection in a water distribution system using the ensemble kalman filter." *Journal of Water Resources Planning and Management*, 147(7).

Chen, Z., Xu, T., Gómez-Hernández, J. J., and Zanini, A. (2021). "Contaminant spill in a sandbox with non-gaussian conductivities: Simultaneous identification by the restart normal-score ensemble kalman filter." *Mathematical Geosciences*, 53(7), 1587–1615.

Civita, M., Gregoretti, F., Morisi, A., Olivero, G., Peano, G., Vigna, B., Villavecchia, E., and Vittone, F. (1990). *Atti della stazione scientifica di della Grotta di Bossea*, Vol. 23. Gruppo Speleologico Alpi Marittime C.A.I. Cuneo - Dipartimento Georisorse e Territorio del Politecnico di Torino, Savigliano.

Emerick, A. A. (2019). "Analysis of geometric selection of the data-error covariance inflation for es-mda." *Journal of Petroleum Science and Engineering*, 182, 106168.

Emerick, A. A. and Reynolds, A. C. (2013). "Ensemble smoother with multiple data assimilation." *Computers & Geosciences*, 55, 3–15.

Evensen, G. (1994). "Sequential data assimilation with a nonlinear quasi-geostrophic model using monte carlo methods to forecast error statistics." *JOURNAL OF GEOPHYSICAL RESEARCH*, 99(C5), 10143.

Evensen, G. (2003). "The ensemble kalman filter: theoretical formulation and practical implementation." *Ocean Dynamics*, 53(4), 343–367.

Evensen, G. (2018). "Analysis of iterative ensemble smoothers for solving inverse problems." *Computational Geosciences*, 22(3), 885–908.

Gassman, P., Reyes, M., Green, C., and Arnold, J. (2007). "Soil and water assessment tool: Historical development, applications, and future research directions, the." *Transactions of the ASABE*, 50(4), 1211–1250.

Gómez-Hernández, J. J. and Xu, T. (2022). "Contaminant source identification in aquifers: a critical view." *Mathematical Geosciences*, 54(2), 437–458.

Hartmann, A., Goldscheider, N., Wagener, T., Lange, J., and Weiler, M. (2015). "Karst water resources in a changing world: Review of hydrological modeling approaches." *Reviews of Geophysics*, 22(7), 2018–242.

Jódar, J., González-Ramón, A., Martos-Rosillo, S., Heredia, J., Herrera, C., Urrutia, J., Caballero, Y., Zabaleta, A., Antigüedad, I., Custodio, E., and Lambán, L. J. (2020). "Snowmelt as a determinant factor in the hydrogeological behaviour of high mountain karst aquifers: The garcés karst system, central pyrenees (spain)." *Science of The Total Environment*, 748, 141363.

Khaki, M., Ait-El-Fquih, B., and Hoteit, I. (2020). "Calibrating land hydrological models and enhancing their forecasting skills using an ensemble kalman filter with one-step-ahead smoothing." *Journal of Hydrology*, 584, 124708.

Kuichling, E. (1889). "The relation between the rainfall and the discharge of sewers in populous districts." *Transactions of ASCE*, 20, 1–56.

Li, N., McLaughlin, D., Kinzelbach, W., Li, W., and Dong, X. (2015). "Using an ensemble smoother to evaluate parameter uncertainty of an integrated hydrological model of yanqi basin." *Journal of Hydrology*, 529, 146–158.

Liang, X., Zheng, X., Zhang, S., Wu, G., Dai, Y., and Li, Y. (2012). "Maximum likelihood estimation of inflation factors on error covariance matrices for ensemble kalman filter assimilation." *Quarterly Journal of the Royal Meteorological Society*, 263–273.

Lucianetti, G., Penna, D., Mastrorillo, L., and Mazza, R. (2020). "The role of snowmelt on the spatio-temporal variability of spring recharge in a dolomitic mountain group, italian alps." *Water*, 12(8), 2256.

Nash, J. E. and Sutcliffe, J. V. (1970). "River flow forecasting through conceptual models part i — a discussion of principles." *Journal of Hydrology*, 10(3), 282–290.

Oaida, C. M., Reager, J. T., Andreadis, K. M., David, C. H., Levoe, S. R., Painter, T. H., Bormann, K. J., Trangsrud, A. R., Girotto, M., and Famiglietti, J. S. (2019). "A high-resolution data assimilation framework for snow water equivalent estimation across the western united states and validation with the airborne snow observatory." *Journal of Hydrometeorology*, 20(3), 357–378.

Rafiee, J. and Reynolds, A. C. (2017). "Theoretical and efficient practical procedures for the generation of inflation factors for es-mda." *Inverse Problems*, 33(11), 115003.

Sherman, L. (1932). "Stream flow from rainfall by the unit graph method." *Engineering News Record*, 501–502.

Shokri, A., Walker, J., van Dijk, A., and Pauwels, V. (2018). "Performance of different ensemble kalman filter structures to assimilate grace terrestrial water storage estimates into a high-resolution hydrological model: A synthetic study." *Water Resuorces Research*, 54(11), 8931–8951.

Sun, Y., Bao, W., Valk, K., Brauer, C. C., Sumihar, J., and Weerts, A. H. (2020). "Improving forecast skill of lowland hydrological models using ensemble kalman filter and unscented kalman filter."

Water Resources Research, 56(8).

Todaro, V., D'Oria, M., Tanda, M. G., and Gómez-Hernández, J. J. (2019). "Ensemble smoother with multiple data assimilation for reverse flow routing." *Computers & Geosciences*, 131, 32–40.

Uwamahoro, S., Liu, T., Nzabarinda, V., Habumugisha, J. M., Habumugisha, T., Harerimana, B., and Bao, A. (2021). "Modifications to snow-melting and flooding processes in the hydrological model—a case study in issyk-kul, kyrgyzstan." *Atmosphere*, 12(12), 1580.

Van Leeuwen, P. J. and Evensen, G. (1996). "Data assimilation and inverse methods in terms of a probabilistic formulation." *Monthly weather review*, 124(12), 2898–2913.

Wang, X. and Bishop, C. H. (2003). "A comparison of breeding and ensemble transform kalman filter ensemble forecast schemes." *Journal of atmospheric sciences*, 60(9), 1140–1158.

White, W. B. (2003). "Conceptual models for carbonate aquifers." *Speleogenesis*, 50(2), 180–186.

Xu, T. and Gómez-Hernández, J. J. (2016). "Joint identification of contaminant source location, initial release time and initial solute concentration in an aquifer via enseble kalman filtering." *WATER RESOURCES RESEARCH*, 52(8), 6587–6595.

Xu, T., Gómez-Hernández, J. J., Zhou, H., and Li, L. (2013). "The power of transient piezometric head data in inverse modeling: An application of the localized normal-score enkf with covariance inflation in a heterogenous bimodal hydraulic conductivity field." *Advances in Water Resources*, 54, 100–118.

List of Tables

1 Performance indicators for the spring 2012 event 25

2 NSE and volume errors for the forecasted spring 2013 flood event. 26

3 NSE and volume errors for the forecasted fall 2016 flood event. 27

Table 1. Performance indicators for the spring 2012 event

Bias (L s^{-1})	−3.15
RMSE (L s^{-1})	13.86
Mean Absolute Error (L s^{-1})	7.92
NSE	0.97
Error in total discharge volume (%)	−2

Table 2. NSE and volume errors for the forecasted spring 2013 flood event.

Spring 2013 forecast	$\chi - std$	χ	$\chi + std$
NSE	0.60	0.72	0.41
Volume error [%]	−27.98	1.84	31.65
Difference between real volume and estimated volume [$m^3 \cdot 10^3$]	998.750	−65.519	−1129.789

Table 3. NSE and volume errors for the forecasted fall 2016 flood event.

Fall 2016 forecast	$\chi - std$	χ	$\chi + std$
NSE	0.52	0.86	0.25
Volume error [%]	−45.56	6.29	59.70
Difference between real volume and estimated volume [$m^3 \cdot 10^3$]	741.647	−102.327	−971.771

List of Figures

1 Fallen snow and estimated snow melting. 29

2 Data collected for the flood event in spring 2012. 30

3 Map of the study area. 31

4 Initial ensembles of IUHs and infiltration coefficients. 32

5 Final IUHs and infiltration coefficients 33

6 Predicted discharges. In yellow, the predictions with the 1000 members of the final ensemble of parameters, and in red, the average of these predictions. 34

7 RMSE (Root Mean Square Error) and ratio RMSE/ES (Ensemble Spread). 35

8 Mean of the IUHs obtained for the spring events and the overall average response, in red. 36

9 Mean of the IUHs obtained for the summer/fall events and the overall average response, in red. 37

10 Yearly values of infiltration 38

11 Example of reconstructed event dating back to spring 2013. 39

12 Example of reconstructed event dating back to spring 2016. 40

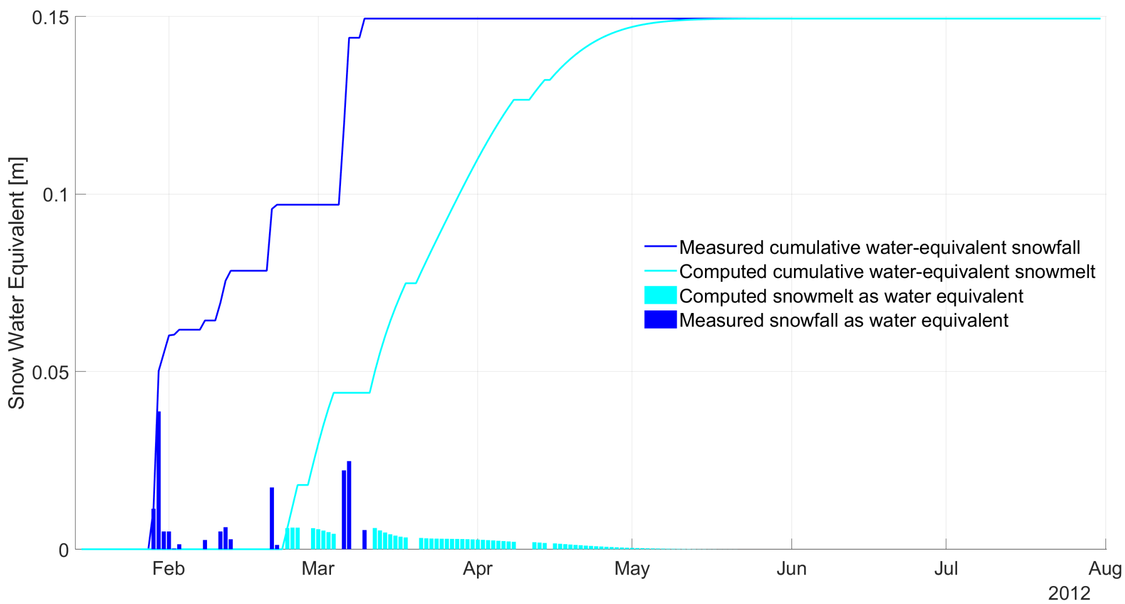

Figure 1. Fallen snow (dark blue) and estimated snow melting (light blue).

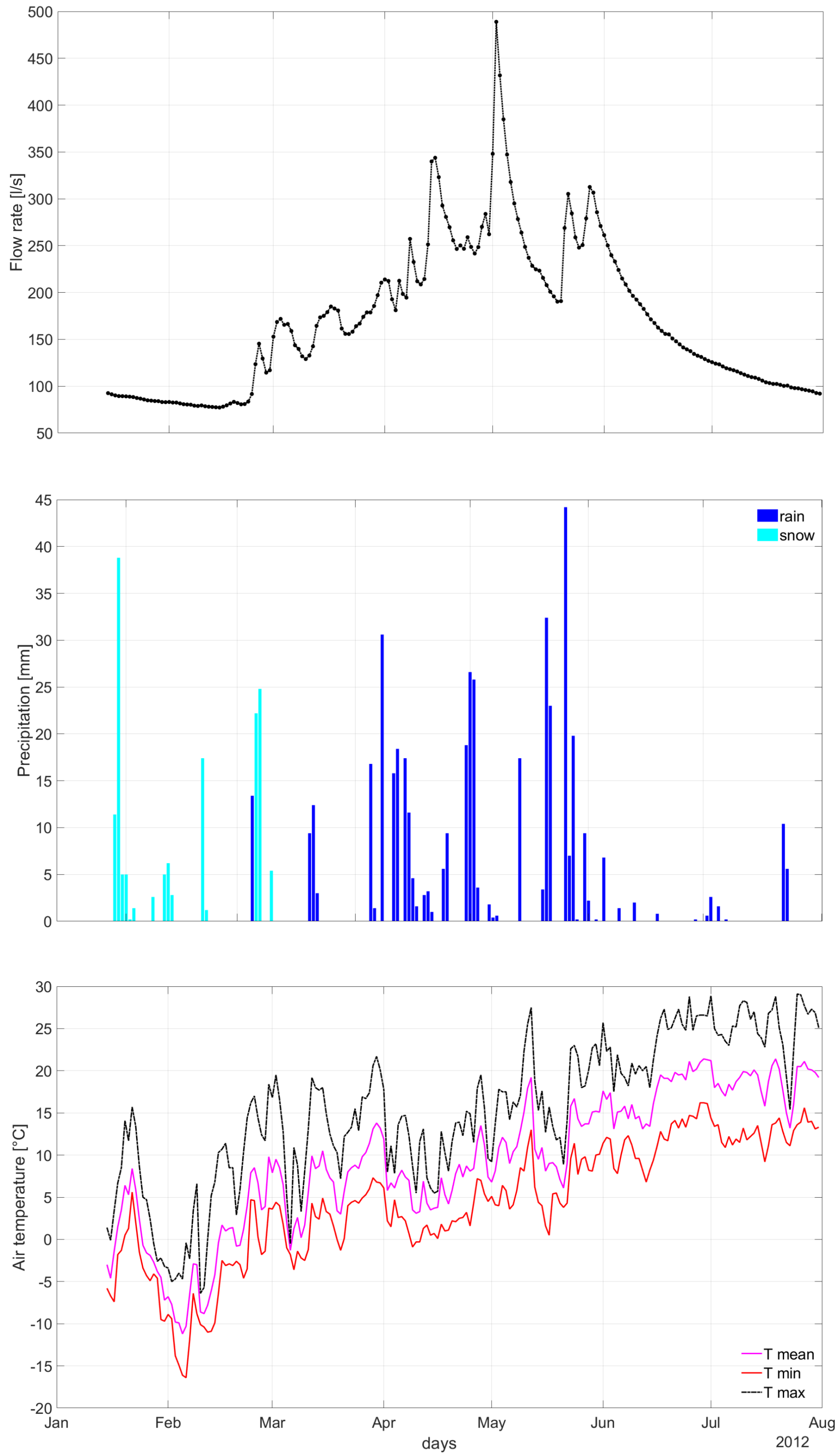

Figure 2. Data collected for the flood event in spring 2012.

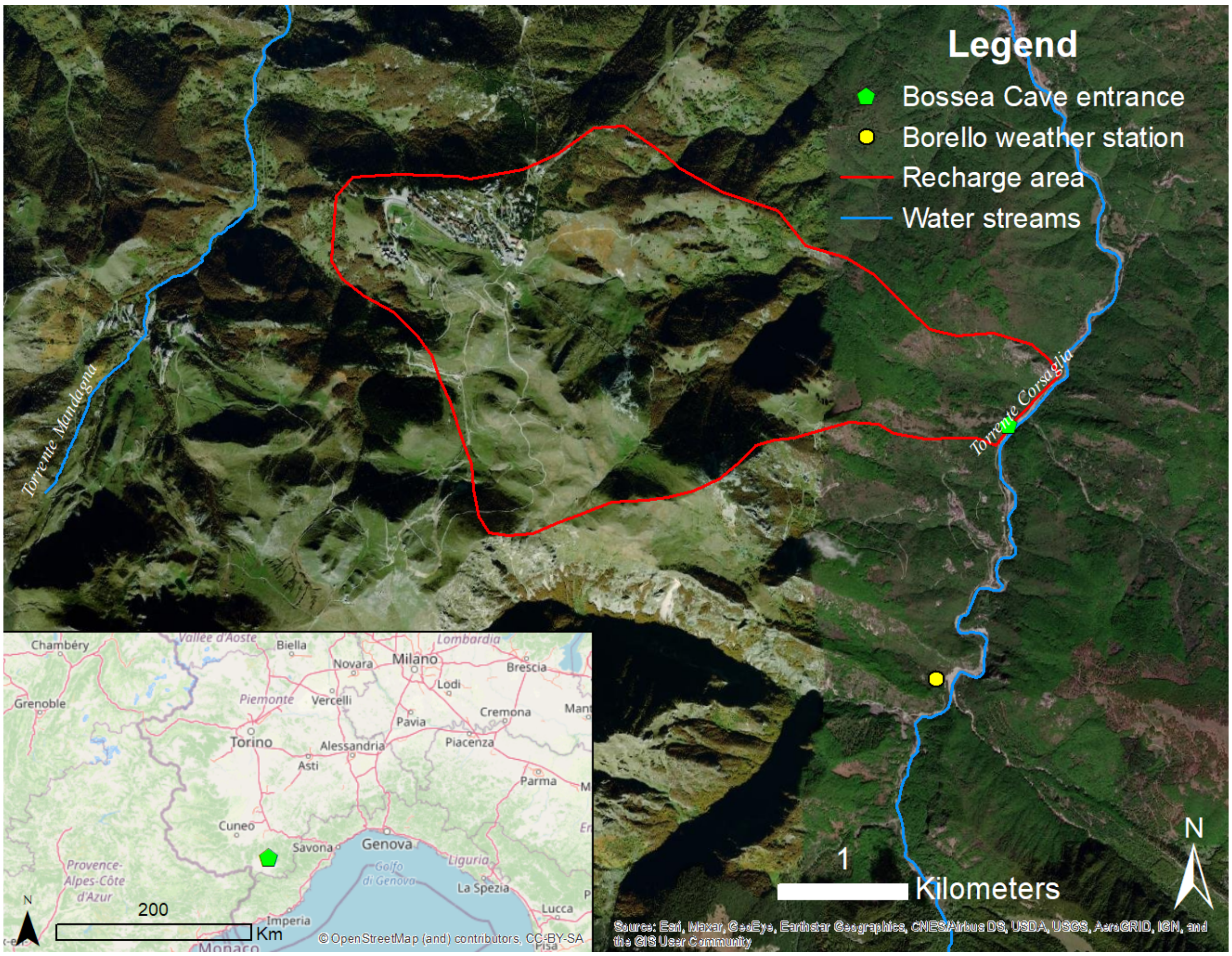

Figure 3. Map of the study area. The aquifer basin, the Bossea cave entrance, and the Borello weather station are shown. The flow rates are measured inside the Bossea cave close to the entrance, and the weather data, at the Borello station.

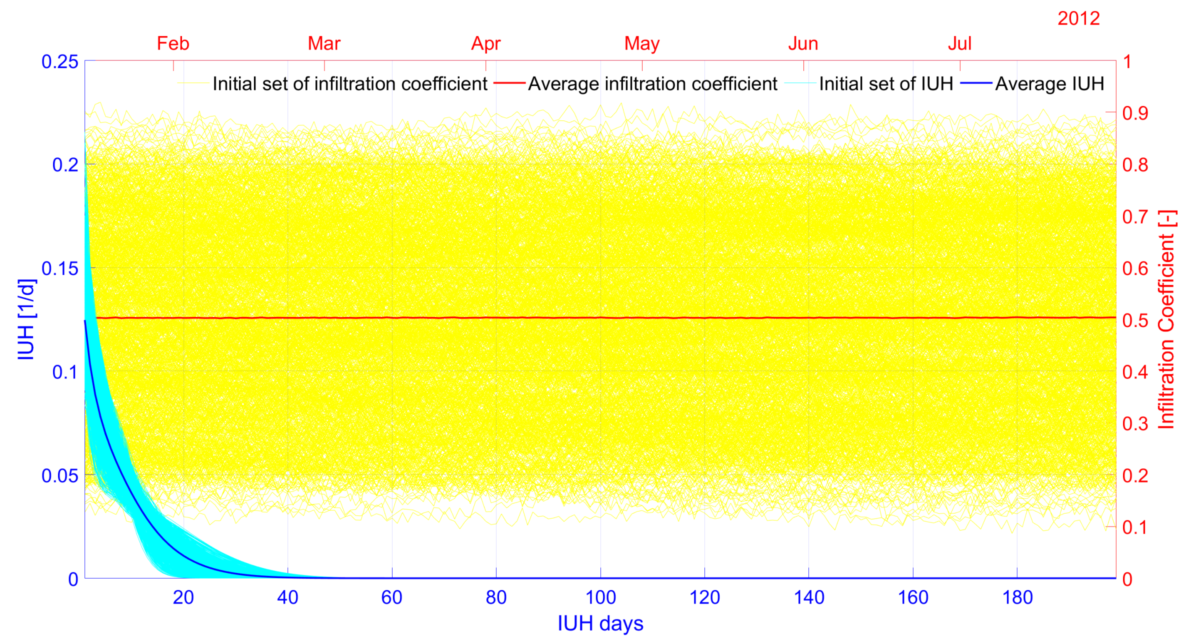

Figure 4. Initial ensembles of IUHs and infiltration coefficients.

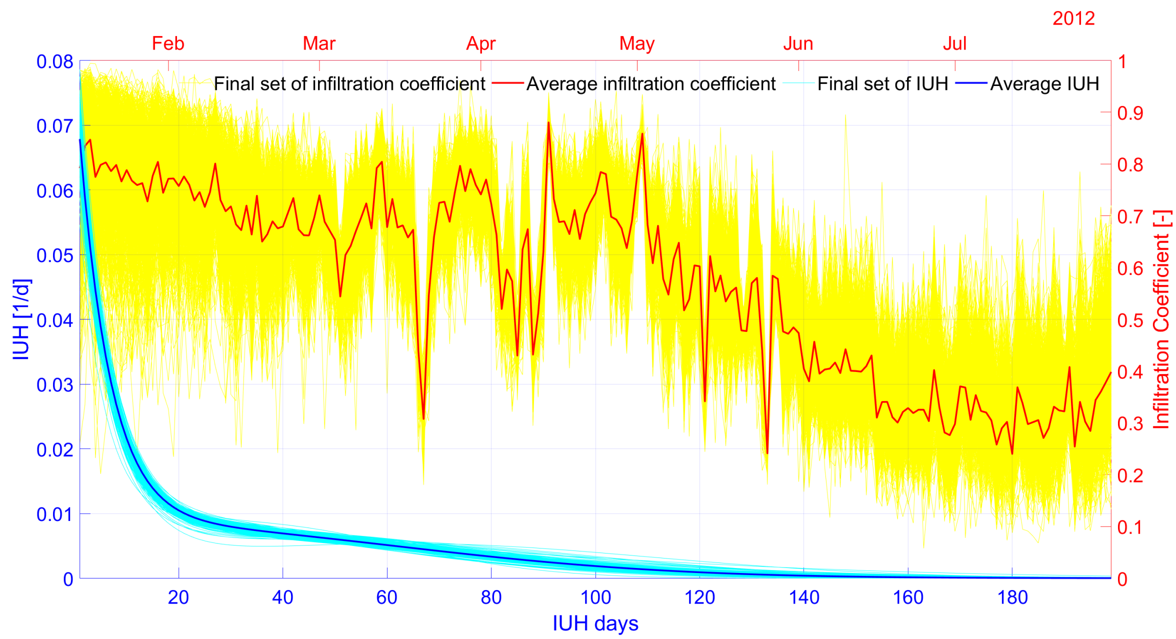

Figure 5. Final IUHs and infiltration coefficients. In light blue the ensemble of 1000 final IUHs, with its mean in dark blue. In yellow the ensemble of infiltration coefficient curves, with its mean in red.

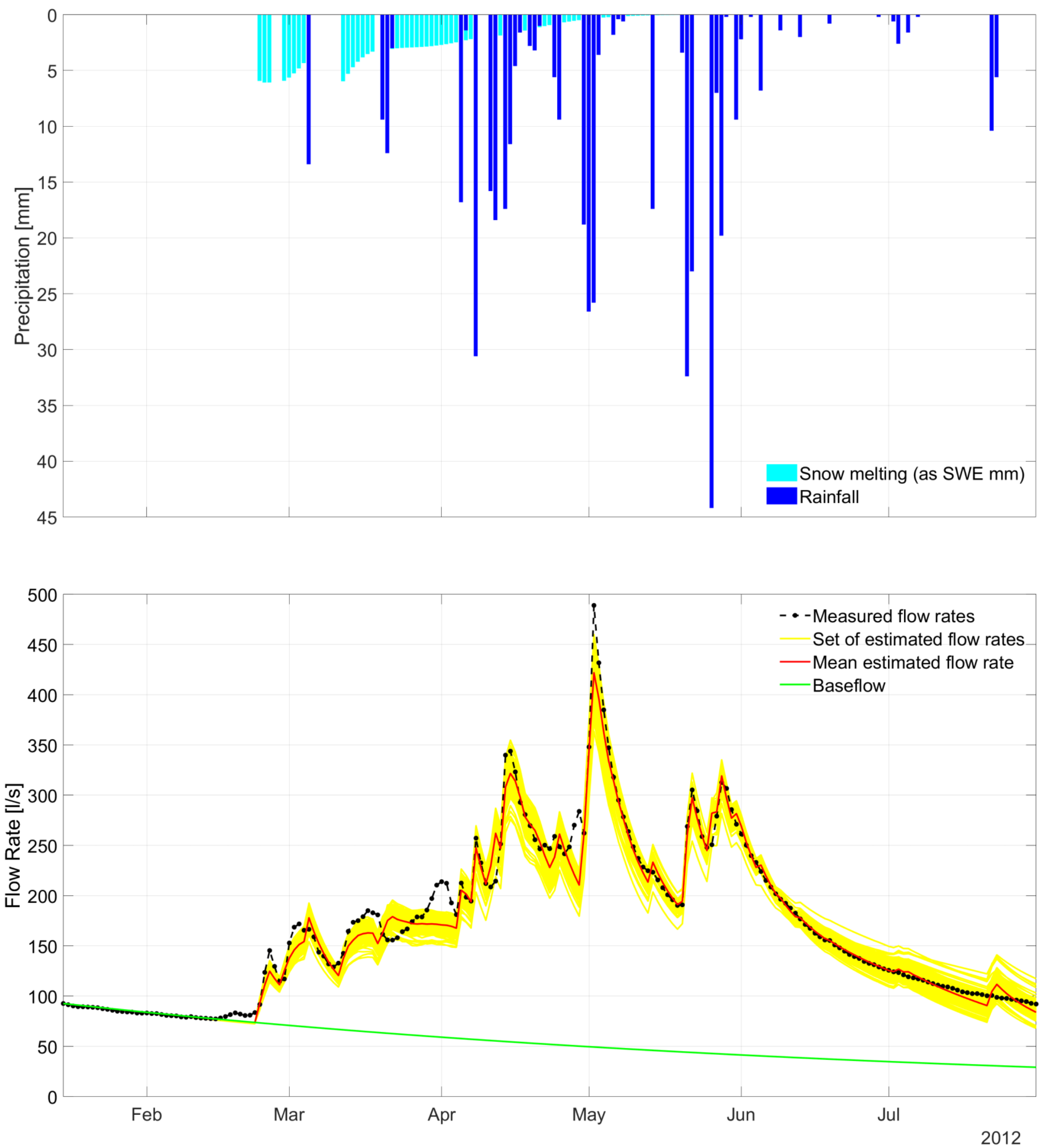

Figure 6. Predicted discharges. In yellow, the predictions with the 1000 members of the final ensemble of parameters, and in red, the average of these predictions. Also shown, the base flow computed with the median of the ensemble base flow parameters, and the snow water equivalent computed with the median of the parameters of the water equivalent model.

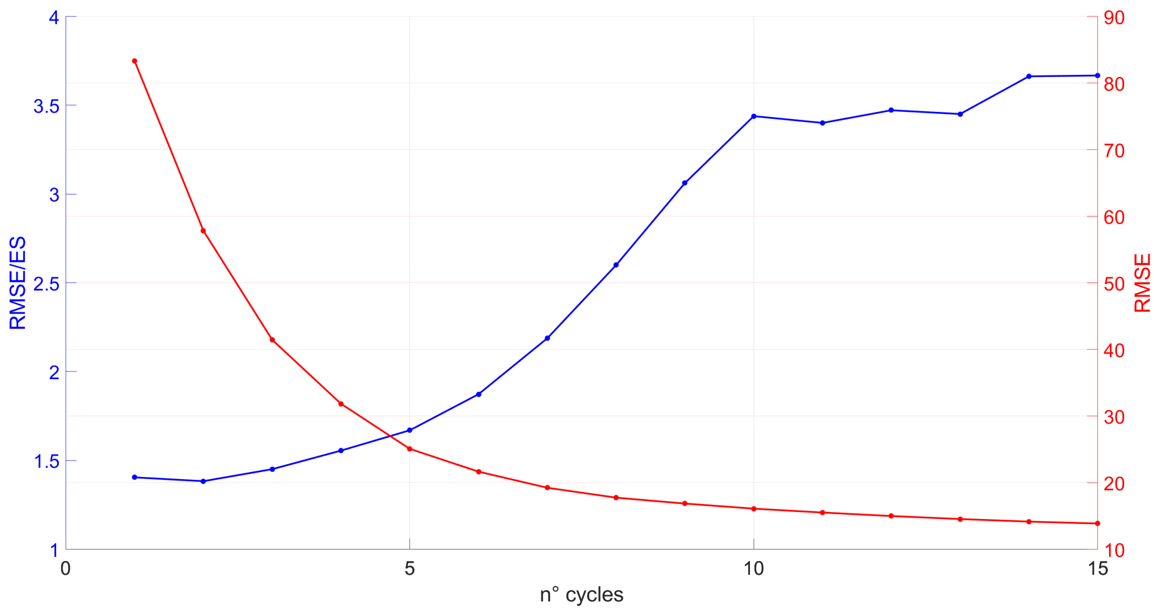

Figure 7. Evolution with the number of data assimilation cycles of the Root Mean Square Error (RMSE) and the ratio RMSE to Ensemble Spread (ES).

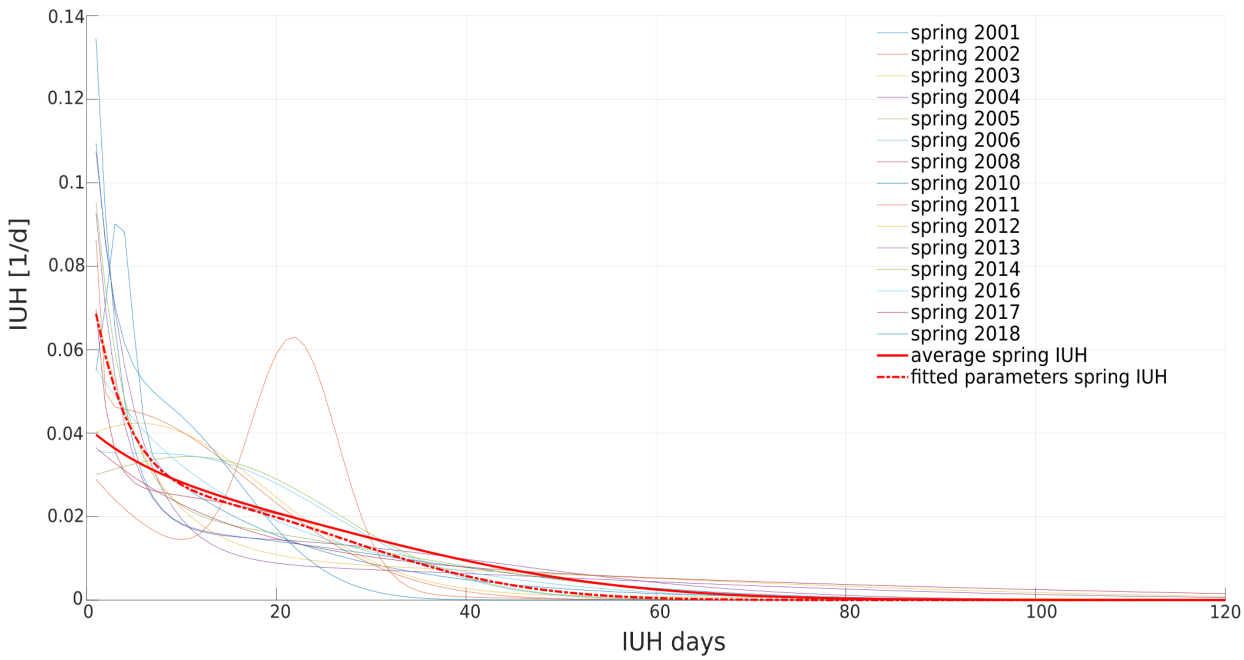

Figure 8. The mean of the IUHs obtained for all the spring events and the two alternative average values: in solid red, the IUH computed with the average parameters, and in dashed red, the parametric curve fitted to the average of the event IUHs.

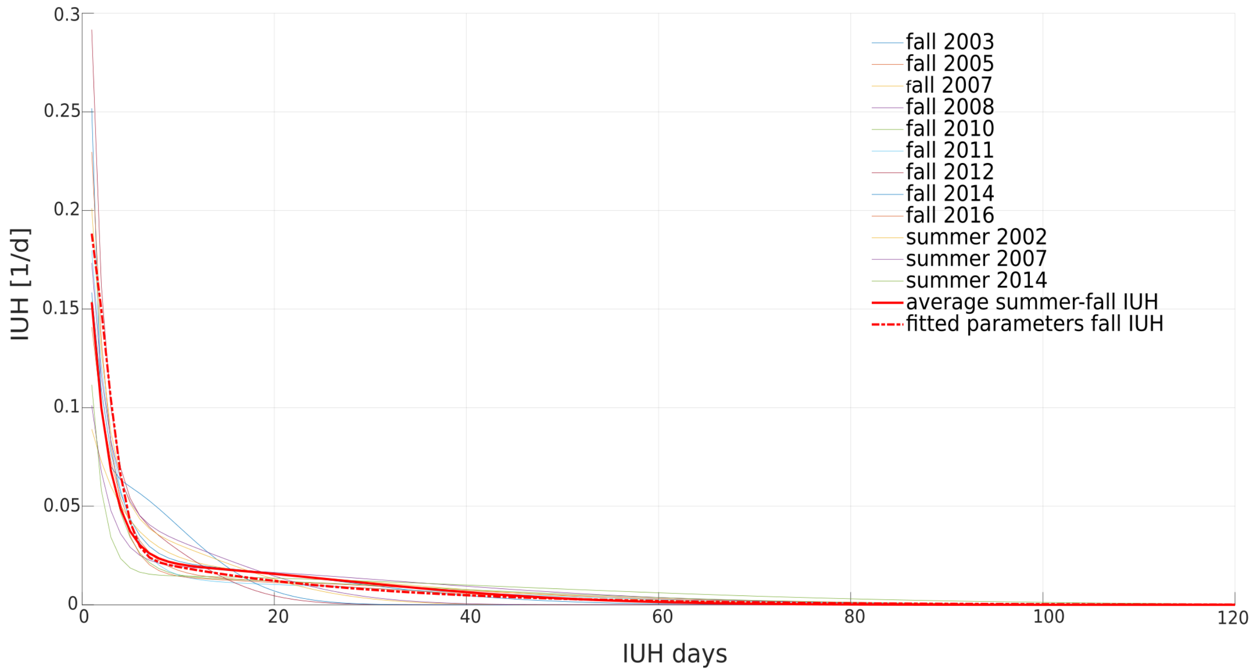

Figure 9. Mean of the IUHs obtained for all the summer/fall events and the two alternative average values: in solid red, the IUH computed with the average parameters, and in dashed red, the parametric curve fitted to the average of the event IUHs.

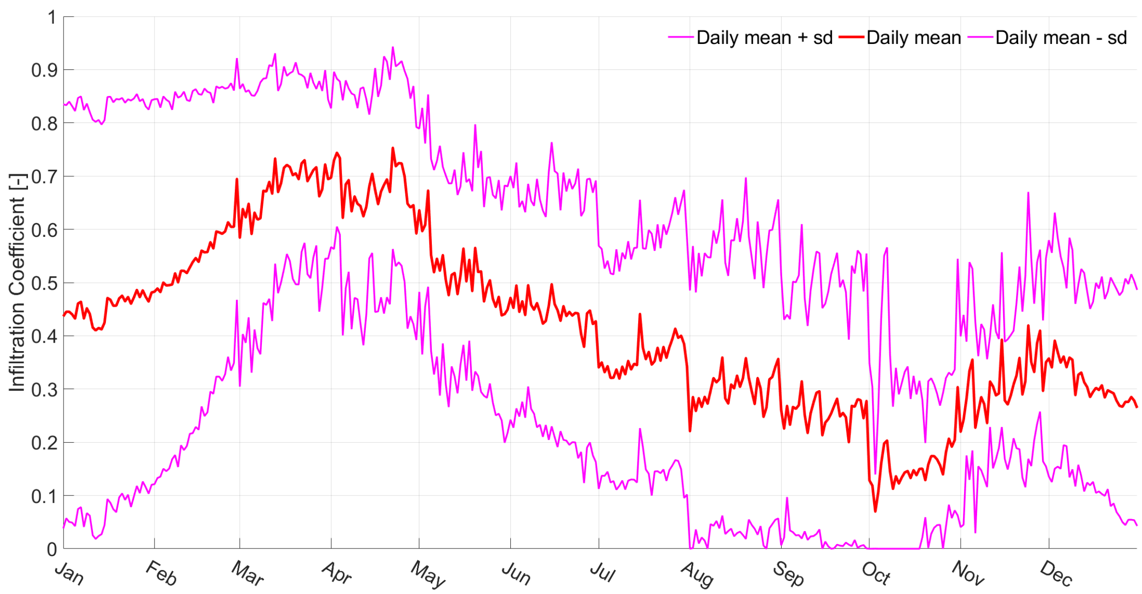

Figure 10. Daily infiltration coefficients. In red, the average value of the coefficients computed over all events, and in blue the uncertainty band of one-standard deviation width.

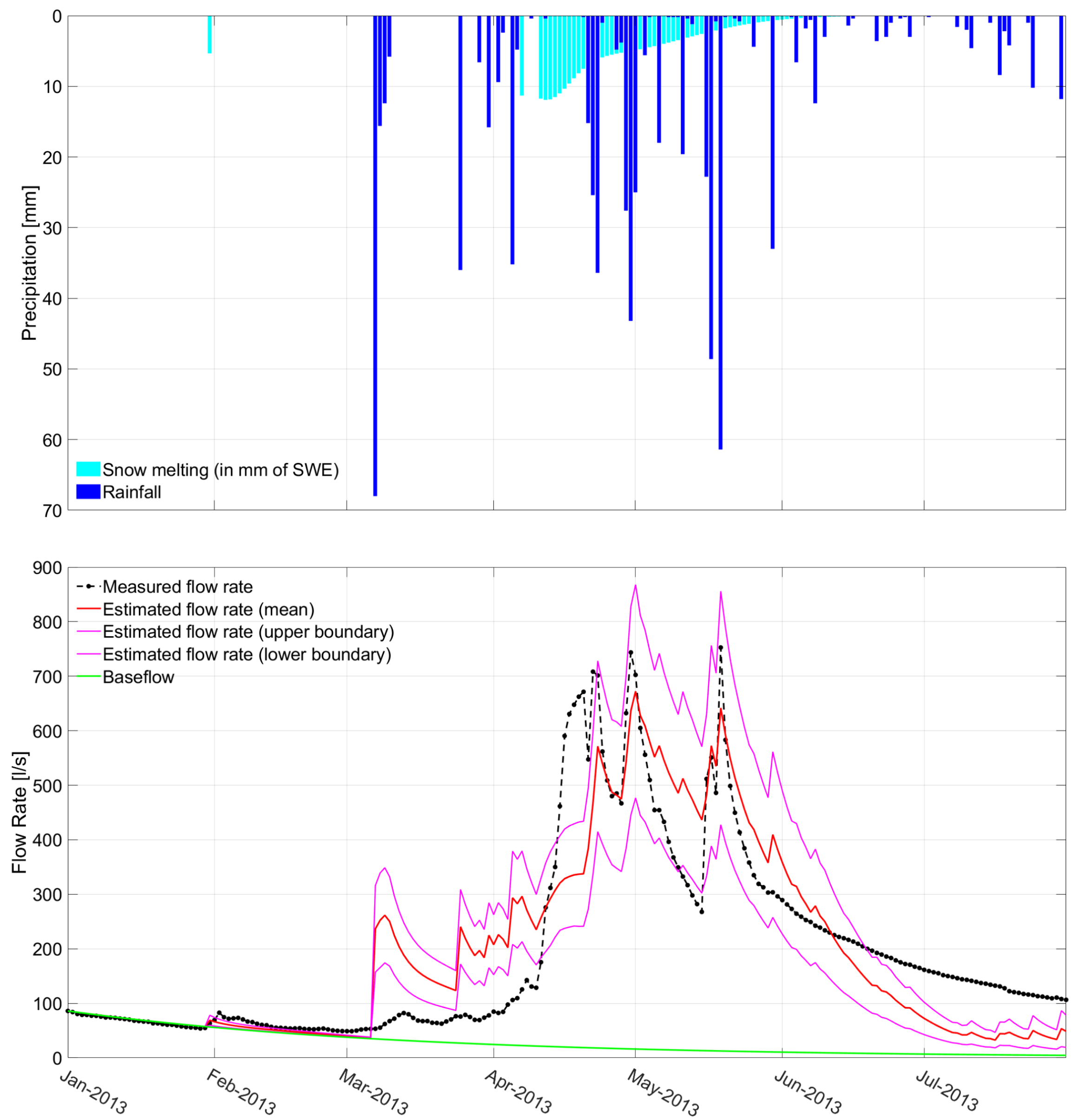

Figure 11. Blind forecast of the spring 2013 event. The black dotted line is the observed discharge, the solid red line is the prediction with the average model, and the two purple lines are the predictions using the infiltration coefficients in the band's limits shown in Fig. 10. For completeness, rain and snow equivalent infiltration, and base flow are also shown.

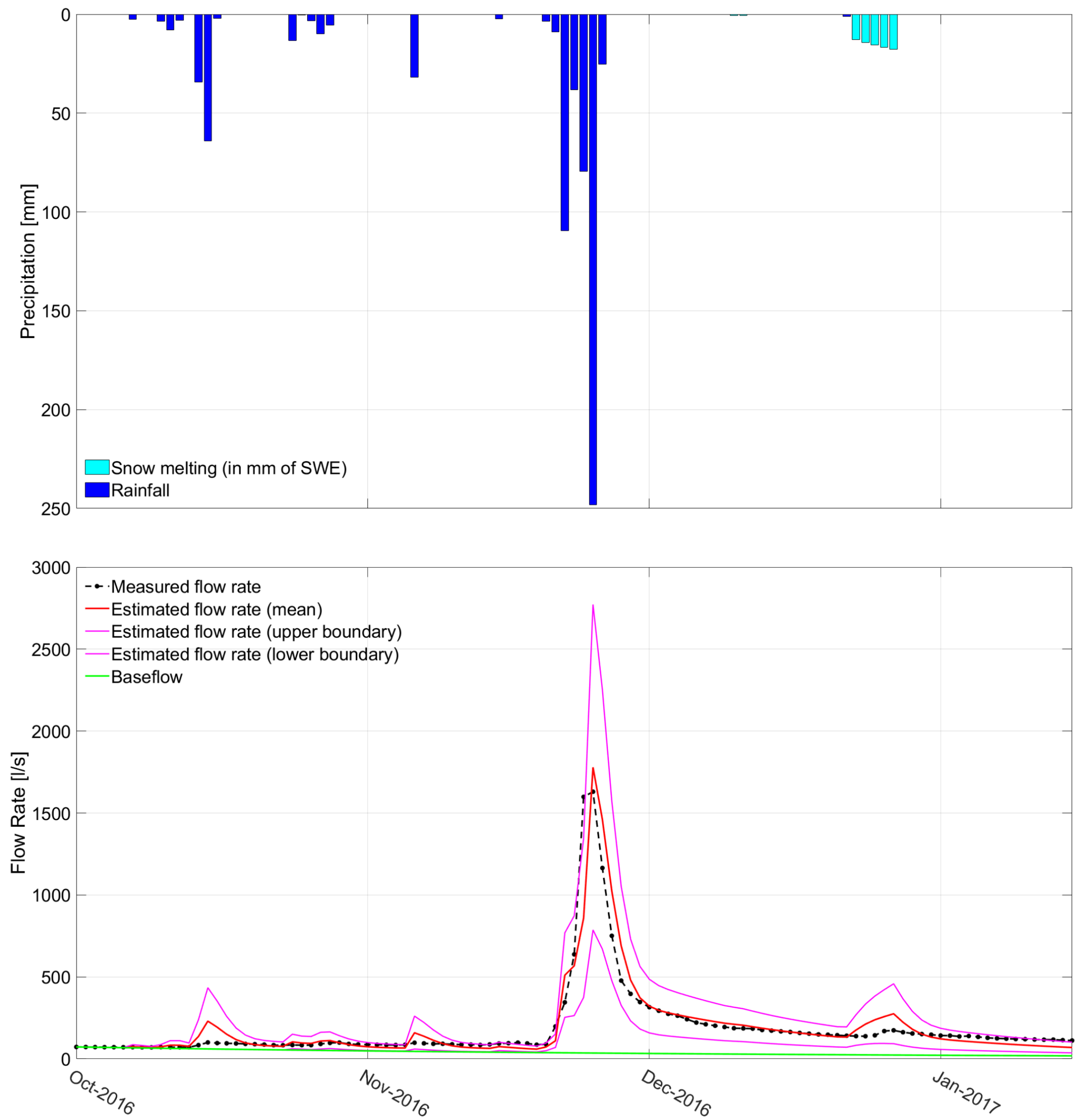

Figure 12. Blind forecast of the fall 2016 event. The black dotted line is the observed discharge, the solid red line is the prediction with the average model, and the two purple lines are the predictions using the infiltration coefficients in the band's limits shown in Fig. 10. For completeness, rain and snow equivalent infiltration, and base flow are also shown.